分类号 _____ 密级 _____

UDC _____ 编号 _____

中国科学院
博士后研究报告

黑洞X射线双星吸积流变化研究

鄢淑平

合作导师 纪丽 研究员

工作完成日期 2014年8月—2018年1月

报告提交日期 2018年1月

中国科学院紫金山天文台

2018年1月

Typeset by LaTeX 2ε at February 6, 2018

With package PostDocRep v0.1e of CTEX.ORG

黑洞X射线双星吸积流变化研究

A Study on Variability from Accretion Flow of a Black Hole X-ray Binary

博士后姓名 鄢淑平

合作导师 纪丽 研究员

流动站（一级学科）名称 天文学

专　业（二级学科）名称 天体物理

研究工作起始时间 **2014年8月**

研究工作期满时间 **2018年1月**

单位名称 中国科学院紫金山天文台

报告提交日期 **2018年1月**

摘　　要

时变分析是对于研究X射线双星吸积物理很重要。然而，很难确定不同吸积流成分的X射线变化。我们提出了几个时变分析方法，并把这些方法应用到黑洞双星GRS 1915+105的“心跳”态，以研究X射线变化起源和盘冕相互作用。

我们通过能量-频率-功率图研究X射线变化起源，并结合相位延迟谱研究盘冕相互作用。在低硬的“缓慢上升”阶段，吸积盘处于局部爱丁顿状态，大部分不规则变化源自冕，并且冕的不规则变化诱导盘的不规则变化。在高软的“爆发”的上升阶段，吸积盘处于辐射压不稳定状态，低频的吸积盘不规则变化显著增强并传播到冕。

我们通过比较幅度比值谱拐折能量来研究不同时标的吸积盘不规则变化的产生区域。在“缓慢上升”阶段，高频和低频幅度比值谱拐折能量很接近，表明这些吸积盘不规则变化源自吸积盘的相同半径，并进一步表明冕对整个吸积盘X射线辐射区产生了作用，因为高频吸积盘不规则变化应该只能来自盘冕相互作用。在“爆发”以及“爆发”之后的阶段，高频拐折能量低于低频拐折能量，说明没有探测到冕对吸积盘最内区的作用。

能量–频率–相位延迟图表明主要产生低频变化的吸积盘总是驱动冕。而在冕变化驱动吸积盘变化时，表明被诱导产生的吸积盘的不规则变化频率范围窄于起诱导作用的冕的变化频率范围。

关键词： 吸积，吸积盘，黑洞物理，X射线双星

Abstract

Timing analysis is crucial for studying the accretion physics of X-ray binaries. It is difficult, however, to associate the different variability components with each spectral component of the accretion flow. We proposed several timing methods and applied them to two RXTE observations of the black hole binary GRS 1915+105 during its heartbeat state to explore the origin of the X-ray variability and the disc-corona interaction.

We study the origin of the X-ray variability through the energy-frequency-power maps and combined them with the phase-lag spectra to investigate the disc-corona interaction. In the low/hard slow rise phase, which corresponds to a local Eddington limit disc, most of the aperiodic variability is produced in the corona, and the corona aperiodic variability induce the disc aperiodic variability. In the high/soft rise phase of the pulse, which corresponds to a radiation pressure instability in the disk, the low-frequency disc aperiodic variability is enhanced significantly and propagates into the corona.

We analyse the formation regions of the disc aperiodic variabilities with different time-scales via comparing the corresponding transition energies of the amplitude-ratio spectra. In the slow rise phase, the transition energies of the low- and high-frequency amplitude-ratio spectra are similar, suggesting that these disc variabilities originate from similar disc radii, and that the whole X-ray radiation region of the disc may be influenced by the corona since the high-frequency disc variability should only result from the disc – corona interaction. In the pulse and post-pulse phases, the high-frequency transition energy is lower than the low-frequency one, showing that we have not detected the effect of the corona upon the innermost part of the disc.

The energy – frequency – phase-lag maps show that the disc, which is dominated by the low-frequency variability, always drives the corona, and the frequency range of the induced disc variability is narrower than that of the inducing corona variability when the corona variability drives the disc variability.

Keywords: accretion, accretion discs; black hole physics; X-rays: binaries

目　　录

表　　格

插　　图

第一章　介绍

1.1　黑洞X射线双星吸积流简介

X射线双星系统是用来研究吸积物理的重要天体。X射线双星的致密星吸积伴星物质，形成环绕致密星的吸积流并辐射X射线。目前已证认的X射线双星系统超过300个[1, 2]。黑洞X射线双星是X 射线双星的亚类，其中的致密星为黑洞。

黑洞X射线双星吸积流包含复杂的成分。首先，其X射线能谱通常包含软成分与硬成分。软成分主要分布在能量较低的软X射线能段。硬成分主要分布在能量较高的硬X射线能段。软成分可能来自几何薄、光学厚的Shakura & Sunyaev类吸积盘[3]。硬成分可能来自高能电子对软X射线光子的逆康普顿散射[4]。康普顿区域的（热的或非热的）高能电子气体通常被称为冕。来自冕的硬X 射线照射吸积盘会产生反射成分[5, 6]。另外，有些黑洞X射线双星也产生喷流[7]和吸积盘风[8, 9]。

1.2　黑洞吸积领域的前沿问题

尽管经过数十年的大量研究，黑洞吸积领域仍然存在很多没有解决的基本问题，如冕的几何与物理性质、硬X射线的辐射机制、喷流和吸积盘风的产生机制等[10]。冕可能是吸积盘截断半径以内的准球状的热吸积流[11]，也可能是覆盖在吸积盘上的非热康普顿气体[12]，或是吸积盘上数量有限的康普顿气体团块[13]。硬X射线可能是冕对软X射线的逆康普顿散射所致[4]，也可能是喷流中高能电子的同步辐射所产生[14, 15]。喷流的产生可能与黑洞自转相关[16]，也可能与吸积盘相关[17]。吸积盘风的产生可能是受热压驱动[18]，也可能是受磁场驱动[19]。

1.3　时变分析–解决问题的潜在重要途径

对于上述前沿问题的研究，时变分析是能谱分析和数值模拟等主要分析手段之外的重要研究角度。常用的时变分析工具是傅里叶变换。对X射线光变

曲线进行傅里叶变换可得功率密度谱[20]和相位/时间延迟谱[21]。图1 为功率密度谱示例。功率密度谱上有时出现显著的峰。这样的峰被称为准周期振荡（QPO），反映吸积流X射线辐射的准周期变化。功率密度谱中扣除QPO之后的部分被称为连续谱（也叫噪声；不同于能谱的连续谱），反映吸积流X 射线辐射的不规则变化。一定特征的能谱反映一定特征的吸积流结构，同时一定特征的功率密度谱对应一定特征的能谱[22]。这种一一对应关系表明，时变分析能够提供能谱分析给出的部分信息，从而能和能谱分析相互印证。时变分析更重要意义在于能够提供能谱分析无法给出的信息，正如超声波探测能够给出其他手段无法探测的金属内部结构的信息。如果时变分析能给出吸积流各成分X射线辐射变化的频率和幅度信息，将十分有利于确定吸积流各成分的位置、尺度，从而有利于上述问题的解决。

1.4 时变分析方法的困境

然而，时变分析还没有成为如能谱分析、数值模拟一样成熟的分析方法。尽管有大量的时变分析[20, 23]，吸积流复杂X射线变化的起源问题仍是当前重要的开放问题[10]。导致这种状况的原因至少有两点，一是QPO与不规则X射线变化的产生区域难以确定，二是它们产生的物理机制也不甚清楚。这两点使得难以对X射线变化进行建模从而无法像拟合能谱一样拟合功率密度谱。

1.5 我们的研究方法

针对X射线变化的起源问题，我们提出了几个简易、有效的时变分析方法，包括幅度比值谱方法[24]、能量–频率–功率图方法[25]、能量–频率–相位延迟图方法[26]。

幅度比值谱可用来研究QPO和不规则X射线变化产生区域。考虑到吸积流的所有成分（吸积盘和冕等）都会产生不规则X射线变化，而只有某一成分（如吸积盘或冕）会产生QPO，我们将功率密度谱连续谱的幅度谱与QPO的幅度谱相除来显示QPO与不规则X射线变化的产生区域。

图1.1为幅度谱比值分析方法示例。图1.1（b）是黑洞双星GRS 1915+105的一次RXTE观测所得数据中的QPO的幅度谱和不同频率范围的不规则X射线变化的幅度谱。这些幅度谱形状类似，很难识别QPO与不规则变化的幅度谱差异。而将不规则变化的幅度谱除以QPO的幅度谱后，二者的差异显而易见

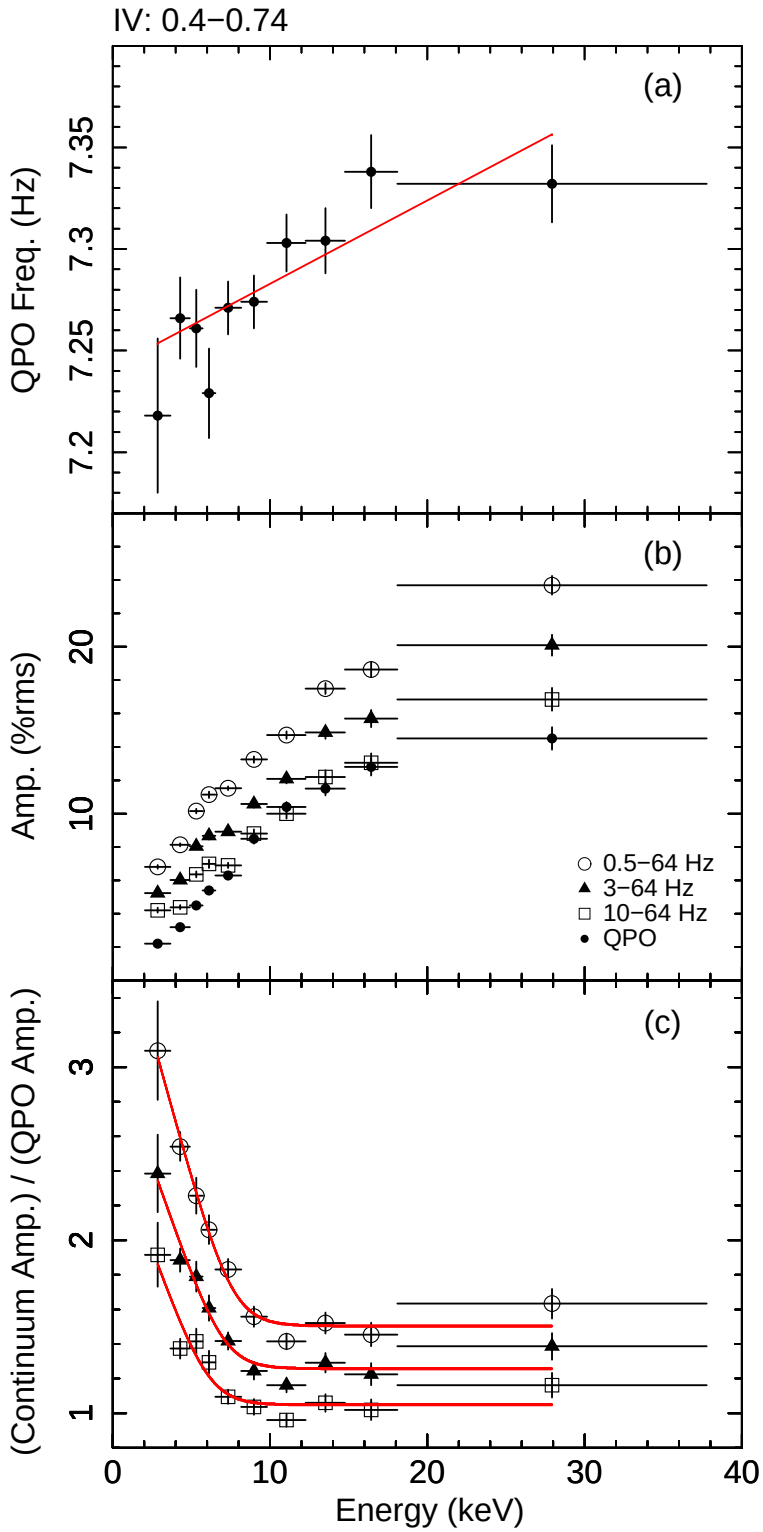

图 1.1: 幅度谱比值分析方法示例（取自[24]）。(a) LFQPO频率谱。(b) 0.5–64 Hz、3–64 Hz、10–64 Hz连续谱rms幅度谱与LFQPO rms幅度谱。(c) 连续谱rms幅度谱与LFQPO rms幅度谱的比值。

（图1.1（c））。可以看出，幅度谱比值在大约10 keV能量处发生拐折。由于吸积盘成分在低于10 keV的能段占主导，冕成分在高于10 keV的能段占主导，所得结果可用QPO源自冕很好地解释。在低于10 keV能段幅度谱比值超出拐折点比值的部分反映吸积盘的不规则变化。显然，10–64 Hz 不规则变化与QPO的幅度谱比值在低能部分有超出，表明有来自吸积盘的高频（高于10 Hz）不规则变化。如果认为如此高频率的不规则变化不可能来自吸积盘而只可能来自冕[11, 21, 27]，那么观测到的吸积盘高频变化可能是由于冕光子对吸积盘的照射所致。

考虑到吸积流不同的成分通常主导不同的能段，为了直观地展示吸积流的不同成分有些什么频率的变化，我们画出X射线变化的傅里叶功率密度在能量和傅里叶频率二维平面上的分布，即**能量-频率-功率图**。通过能量-频率-功率图，可以分析不同频率的X射线变化的起源，即源自吸积流哪个成分。而进一步结合不同能段的X射线变化的相位（时间）延迟谱，即相位延迟–频率关系，就可以研究吸积流不同成分之间的相互作用。而相位延迟在能量和频率二维图上的分布，即**能量-频率-相位延迟图**，对比相位延迟谱能够显示更多相位延迟信息，从而可以用来研究吸积流不同成分之间的相互作用的细节。

1.6 对黑洞双星GRS 1915+105的时变研究

黑洞双星GRS 1915+105是在1992年由$GRANAT$/WATCH探测器发现的低质量黑洞双星系统[28]。它的中心天体是质量为$14 \pm 4 M_{\odot}$、快速自转的黑洞[29–32]。它的伴星是质量为$0.8 \pm 0.5 M_{\odot}$的K-M III型巨星[33, 34]。中心黑洞与伴星距离约为108 ± 4 $R_{\odot}$，轨道周期约为33.5天[35]。它位于银河系内，距离地球$\sim$ 11 kpc[36, 37]。GRS 1915+105被观测到有很强的射电喷流[7, 36]，因而也被称为微类星体。

GRS 1915+105自1992年被发现以来，一直处于爆发的状态，也是目前发现的仅有的具有奇特的、大幅度的、结构性变化的两个源之一。这里所说的奇特的、大幅度的、结构性的变化，指的是源的X射线光度能在秒量级的时间内发生量级的改变，并且这样的光度变化会不断重复发生，持续几小时到几天。这种X射线光度的大幅度结构性变化挑战了当前的吸积理论，对其深入研究将促进吸积理论的发展。

GRS 1915+105的X射线光变曲线尽管非常复杂，仍然可以分为有限的种

类。依据光变曲线的形状和相应的双色图（color–color diagram）的特征，GRS 1915+105所处的态可以分为十余种[38–40]。其中非常特殊的一类是“心跳”态（ρ态）。心跳态因光变曲线类似人的心电图而得名。处于ρ态时，源在光度较低、能谱较硬的态和光度较高、能谱较软的态之间准周期地跃迁。态跃迁发生的时标为几十秒到上百秒。ρ态这样的短时标的、准周期性的态跃迁，非常适于用相位分解方法研究能谱与时变特性的演化，从而适宜于分析X射线变化的起源。

因此，通过应用我们提出的方法（幅度比值谱方法、能量–频率–功率图方法、能量–频率–相位延迟图方法），本文系统的研究GRS 1915+105处于ρ态时的X射线不规则变化和QPO的起源，并为研究吸积流的盘冕相互作用提供了一条新途径。本文第二章介绍了能量–频率–功率图和时间延迟谱的结果以及结合能谱分析得到的能谱和时变相统一图像。第三章介绍了幅度比值谱和能量-频率-相位延迟图的结果。第四章是对以上工作的总结以及后续工作的展望。

第二章　A Timing View of the Heartbeat State of GRS 1915+105

2.1 Introduction

Accretion plays a crucial role in the evolution of black hole binaries (BHBs). Timing analysis is an important tool for studying the accretion flow. The Fast Fourier Transformation is one of the most popular methods of timing analysis. However, the origins of the X-ray aperiodic variabilities and the low-frequency quasi-periodic oscillations (LFQPOs) in Fourier power density spectra (PDS) from BHB accretion flows remain yet unsolved [e.g. 10].

GRS 1915+105 is a BHB suitable for studying the X-ray variability. The source has a rapidly spinning black hole [29, 31, 32, 41] with a mass of $\sim 12\ M_{\odot}$, and a K-M III secondary with a mass of $\sim 0.8\ M_{\odot}$ [33, 34, 42]. It is ~ 10 kpc away from the earth [e.g. 36, 37, 42], and is considered a microquasar because it shows a relativistic jet whose inclination to the line of sight is $\gtrsim 60^{\circ}$ [7, 36, 42]. GRS 1915+105 has been active for more than twenty years [28], and is intensively observed with the *Rossi X-ray Timing Explorer* (*RXTE*). The various kinds of source variabilities [38–40] and the abundance of LFQPOs [e.g. 43–48] displayed in the *RXTE* data make it a unique source for studying the X-ray variability.

The variabilities of GRS 1915+105 are classified into 14 classes based on the count rate and the colour characteristics of the source [38–40]. Each class is regarded as transitions among three states, A, B and C. State C is a low-luminosity, spectrally hard state while states A and B are high-luminosity, soft states. The ρ class (heartbeat state) is a peculiar class where the source oscillates quasi-periodically between states B and C. The light curves in the ρ class have one to several peaks per ρ-cycle [e.g. 38, 49–51]. We call the ρ class with one peak per cycle the single-peaked ρ class (hereafter called ρ_1 class), and the ρ class with two peaks per cycle the double-peaked ρ class (hereafter called ρ_2 class).

Neilsen et al. (2011, 2012) [52, 53] carried out a phase-resolved spectral analysis

of the *RXTE* observations 60405-01-02-00 during the ρ_2 class and 40703-01-07-00 during the ρ_1 class. In order to investigate the origin of the LFQPO, Yan et al. (2013) [24] performed a phase-resolved timing analysis of the ρ_2 class, and showed that the LFQPO was tightly related to the corona. Besides, for one phase interval of the ρ_2 class Yan et al. (2013) [24] first detected a high-frequency ($\gtrsim$ 10 Hz) aperiodic variability from the disk through the amplitude-ratio spectrum method.

In this paper we present the results of the diagram of the power density as a function of Fourier frequency and ρ-cycle phase (phase-frequency-power map), the diagram of the power density as a function of Fourier frequency and photon energy (energy-frequency-power map), and the phase lag as a function of Fourier frequency (phase-lag spectrum) of the ρ_1 and ρ_2 classes. We use the phase-frequency-power maps to investigate the continuous evolution of the X-ray variability along with the spectral evolution, use the energy-frequency-power maps to visually display the correlation between the X-ray variability and the spectral components, and use the phase-lag spectra to obtain the sequence information of the X-ray variabilities from different spectral components.

In addition to studying the origin of the X-ray variability, we aim to acquire a spectral-timing unified picture of the accretion in the heartbeat state of GRS 1915+105 through a combination analysis of our timing results and the spectral results presented by Neilsen et al. (2011, 2012) [52, 53].

We describe the observations and the data reduction methods in Section 2.2, present the results in Section 2.3, show the discussion in Section 2.4, and list the conclusions in Section 2.5.

2.2 Observations and data reduction

Using the phase-folding method of Neilsen et al. (2011) [52], Yan et al. (2013) [24] performed a phase-resolved timing analysis for the ρ_2 class (*RXTE* observation 60405-01-02-00 on 2001 May 23 at 11:18:42 UT with 13.9 ks exposure time). In this paper with the same method we carry out a timing analysis for the ρ_1 class (*RXTE* observation 40703-01-07-00 on 1999 February 26 at 07:32:13 UT with 9.9 ks exposure time). We extract two dead-time-corrected and background subtracted light curves

with a time resolution of 1 s from the binned-mode data (B_8ms_16A_0_35_H_4P) in the 1.9–13.0 keV band and the event-mode data (E_16us_16B_36_1s) in the 13.0–60 keV band respectively, and add them together to obtain a light curve. We apply the barycenter correction to the light curve and then fold it to obtain an average folded light curve. We determine the start time of each cycle by an iterative cross correlation method [for more details see 52], and obtain 209 cycles with a mean period of 44.54 s for the ρ_1 class. In Yan et al. (2013) [24] we obtained 257 cycles with a mean period of 50.29 s for the ρ_2 class. We average the PDS from a certain phase interval of all cycles for each class to study the timing properties of the ρ oscillation, since the shape difference of the individual cycles is always less than 20% for a given phase interval.

We calculate the PDS in different energy bands from the binned and event files using 2 s segments at a time resolution of 8 ms, and subtract the dead-time-corrected Poisson noise (Morgan et al. 1997) from each PDS and normalize them to units of (RMS/mean)^2/Hz [e.g. 54]. We then fit the PDS with a model including several Lorentzians to represent the broad-band noise and the LFQPOs [55, 56]. We calculate the PDS in the 1.9–60 keV band for each 0.04 phase interval of the ρ_1 class, and calculate the PDS in the 2.1–60 keV band for each 0.02 phase interval of the ρ_2 class. We then use these PDS to produce the phase-frequency-power maps for the ρ_1 and ρ_2 classes. We compute the significance of the QPOs with the method adopted by Strohmayer & Watts (2005) [57]. The 3.9 Hz QPO in the phase 0.84–0.86 of the ρ_2 class has the minimum significance of 0.0017 among all of the QPOs studied.

We produce the PDS in different energy bands for phases I (0.00–0.08), II (0.08–0.26), III (0.26–0.40), IV (0.40–0.60), and V (0.60–1.00) of the ρ_1 class, and for phases i (0.02–0.12), ii (0.12–0.26), iii (0.26–0.40), iv (0.40–0.74), v (0.74–0.92), and vi (0.92–0.02) of the ρ_2 class, and use these PDS to produce the energy-frequency-power maps. We correct these PDS for background due to the energy dependence of the background [58, 59].

For these phases we calculate the Fourier cross power spectra of two light curves extracted in different energy bands following Nowak et al. (1999) [21] to obtain the phase-lag spectra. For the ρ_1 class, a positive phase lag denotes that the variability in the 5.1–38.4 keV band lags that in the 1.9–5.1 keV band. For the ρ_2 class, a positive

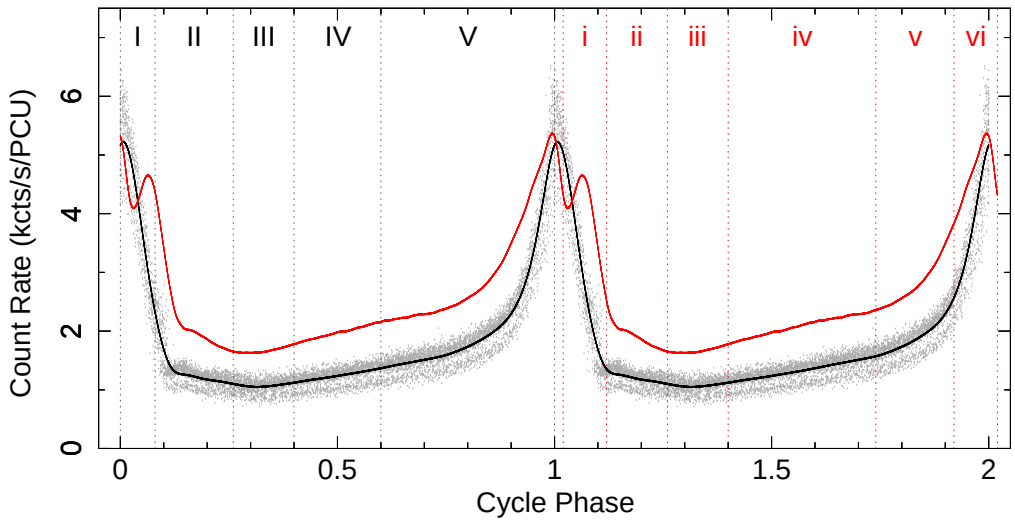

图 2.1: The phase-folded PCA light curves of the ρ_1 class (black; *RXTE* Observation 40703-01-07-00) and the ρ_2 class (red; *RXTE* Observation 60405-01-02-00) in GRS 1915+105. The gray points are the data points of the ρ_1 class. The black and red vertical dashed lines denote phases I (0.00–0.08), II (0.08–0.26), III (0.26–0.40), IV (0.40–0.60), V (0.60–1.00) of the ρ_1 class, and phases i (0.02–0.12), ii (0.12–0.26), iii (0.26–0.40), iv (0.40–0.74), v (0.74–0.92), vi (0.92–0.02) of the ρ_2 class.

phase lag denotes that the variability in the 4.9–37.8 keV band lags that in the 2.1–4.9 keV band. The reference bands for the phase lag calculations for the two classes cannot be the same due to that they were observed in different gain epochs while archived with the same binning modes. All error bars in this paper correspond to 1σ confidence level.

2.3 Results

We present in this section the phase-frequency-power maps, the energy-frequency-power maps, and the phase-lag spectra of the ρ_1 and ρ_2 classes. We show the phase-folded *RXTE*/Proportional Counter Array (PCA) light curves and the ρ-cycle phase divisions of the two ρ classes in Figure 2.1. For the aperiodic variability we define three frequency bands, the low-frequency band ($\lesssim$ 1 Hz), the intermediate-frequency band ($\sim$ 1–10 Hz), and the high-frequency band ($\gtrsim$ 10 Hz).